

Papanikolaou, M. G., Hadjithoma, S., Chatzikypraiou, D. S., Papaioannou, D., Drouza, C., Tsipis, A. C., Miras, H. N. , Keramidas, A. D. and Kabanos, T. A. (2018) Investigation of dioxygen activation by copper(ii)-
iminate/aminato complexes. *Dalton Transactions*, 47(45), pp. 16242-16254.
(doi:[10.1039/c8dt03137a](https://doi.org/10.1039/c8dt03137a)).

This is the author's final accepted version.

There may be differences between this version and the published version.
You are advised to consult the publisher's version if you wish to cite from
it.

<http://eprints.gla.ac.uk/173784/>

Deposited on: 27 November 2018

Enlighten – Research publications by members of the University of Glasgow
<http://eprints.gla.ac.uk>

Ligand mediated dioxygen activation by mononuclear copper(II) complexes: A combined experimental and theoretical study†

Michael G. Papanikolaou,^{§a} Sofia Hadjithoma,^{§b} Dimitra S. Chatzikypraiou,^a Dionysios Papaioannou,^{*c} Chrysoula Drouza,^d Athanassios C. Tsipis,^{*a} Haralampos N. Miras,^{*c} Anastasios D. Keramidas,^{*b} and Themistoklis A. Kabanos^{*a}

^aSection of Inorganic and Analytical Chemistry, Department of Chemistry, University of Ioannina, Ioannina 45110, Greece. E-mail: tkampano@cc.uoi.gr and attsipis@uoi.gr

^bDepartment of Chemistry, University of Cyprus, Nicosia 1678, Cyprus. E-mail: akeramid@ucy.ac.cy

^cLaboratory of Synthetic Organic Chemistry, Department of Chemistry, University of Patras, GR-26504 Patras, Greece. E-mail: dapapaio@upatras.gr

^dDepartment of Agricultural Production Biotechnology and Food Science Cyprus University of Technology Limassol 3036, Cyprus.

^eWest CHEM, School of Chemistry, University of Glasgow, Glasgow G12 8QQ, U.K. E-mail: harism@chem.gla.ac.uk

†Electronic supplementary information (ESI) available. CCDC 1576869, 1576874, 1858742 and 1576873. For ESI and crystallographic data in CIF or other electronic format see DOI:

Keywords: amide ligands, copper, DFT calculations, O₂ activation, X-ray structures

Abstract

The activation of dioxygen by metal ions is critical in chemical and bio-chemical processes. A scientific challenge is the elucidation of the activation site of dioxygen, in some copper metalloproteins, which is either the metal center or the substrate. In an effort to address this challenge, we prepared a series of new copper(II) complexes (**1**·2H₂O, **2**·CH₃OH, **3**) with bio-inspired amidate ligands and investigated their activity towards dioxygen activation. The ligated to the copper(II) secondary amine group of the complex **1**·2H₂O in methyl alcohol is oxidized (2e⁻) by air dioxygen in a stepwise fashion to imine group, giving the complex **2**. The copper(II) complex **2** in methyl alcohol induces the 4e⁻ oxidation of the ligated to copper(II) imine functionality, by air dioxygen, to an azinate group resulting in the isolation of a dinuclearazinate copper(II) compound (**4**). Experimental and theoretical studies including X-band EPR, UV-vis and ESI-MS spectroscopies and density functional theory computations indicate a direct attack of the dioxygen to the ligated to copper(II) –HC=N– group and a possible mechanism of the oxidation of the ligated to copper(II) –HC=N– functionality to an azinate group is provided. This unprecedented dioxygen activation by copper's substrate paves the way for further exploration of the O₂ activation mechanisms in enzymes and development of effective catalysts in the O₂-involved green organic synthesis.

Introduction

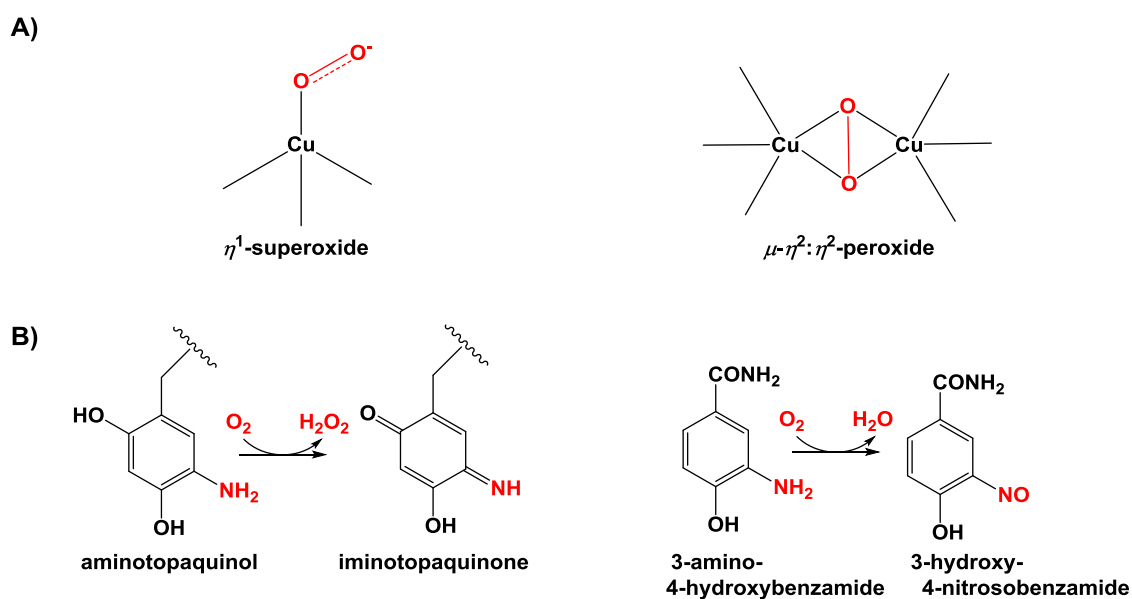
The activation of dioxygen by metal ions¹ is a central reaction in biological,²⁻⁵ catalytic^{6, 7, 8} and energy storage⁹⁻¹² processes. Several copper-based metalloenzymes activate dioxygen in a variety of biological functions,¹³⁻²⁰ such as, the regulation of neurotransmitters, dioxygen transport, and cellular respiration.

Copper is one the most frequently used metals in enzymes to activate dioxygen²⁰⁻²⁵ and thus far, a variety of model copper compounds have been developed to stabilize mononuclear Cu^{II}-superoxide species.²⁶⁻³⁷ The common oxidation states of copper found in biological systems are considered to be I and II, but the last years there is a strong belief that oxidation state III might have potential importance in copper enzymes in biology.³⁸⁻⁴³

Combined enzymatic and model studies have been used to unveil the mechanisms of dioxygen activation by copper proteins.^{5, 25, 44-47} It has been suggested for the most of the copper enzymes that the first step in dioxygen activation is the coordination of dioxygen to copper ion and formation of the metal superoxo species.¹⁸ Although, several modes of dioxygen ligation to copper have been observed in model compounds, only the η^1 -superoxide and the μ - η^2 : η^2 -peroxide modes of ligation have been identified crystallographically in mononuclear and dinuclear copper metalloprotein active sites respectively (Scheme 1A).

An example of η^1 -superoxide mode of ligation has been found in copper amine oxidases (CAOs), which utilize dioxygen to promote aerobic oxidation of primary amines to aldehydes. Mechanistic studies in CAOs and model systems revealed that the reaction proceeds via a transamination pathway; however the mechanism is still a subject of controversy.^{17, 48-51} The electron transfer from aminotopaquinol to dioxygen results in the formation of superoxide which oxidizes imino-topaquinone (Scheme

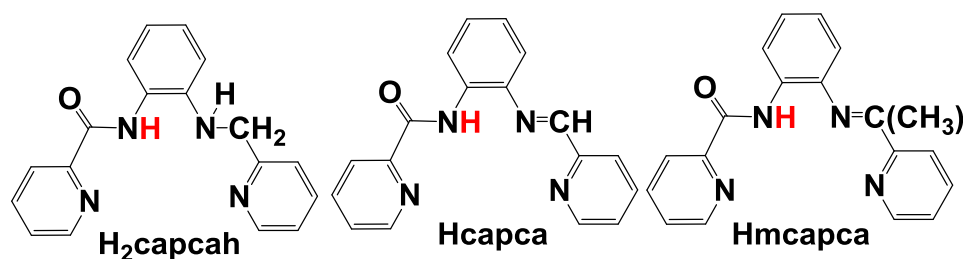
1B).^{17, 50, 52-54} An example of copper enzyme with a $\mu\text{-}\eta^2\text{:}\eta^2$ -peroxide mode of ligation is the recently discovered binuclear copper enzyme NspF, which activates dioxygen to convert 3-amino-4-hydroxybenzamide to 4-hydroxy-3-nitrosobenzamide (Scheme 1B).⁵⁵ The NspF enzyme, like in other copper monooxygenases, reacts with dioxygen to form a $\mu\text{-}\eta^2\text{:}\eta^2$ -peroxide adduct.



Scheme 1 The crystallographically identified modes of dioxygen ligation in copper metalloproteins (A);

In some other copper metalloproteins, the activation site of dioxygen is under debate, and it is either the metal center or the substrate. For example, a mechanism of dioxygen activation that has been proposed for quercetinase,⁵⁶ a copper dioxygenase which breaks down quercetin and other flavonols to depsides, is its direct reaction with the substrate's radical.⁵⁷ Studies on catechol⁵⁸⁻⁶⁰ and *p*-semiquinone^{12, 61} radical metal-complexes, models of oxidases, proved that dioxygen is activated by the ligand's radical and thus, support the proposed mechanism for quercetinase.

In this study, new bioinspired model copper(II) complexes have been employed in order to better understand the O_2 activation mechanism by copper based metalloproteins.⁶² More specifically, the synthesis, the structural and physicochemical characterization of a series of copper(II) compounds with the tetradentateamidate ligands, *N*-{2-[(2-pyridylmethylene)amino]phenyl}pyridine-2-carboxamide (Hcapca, Scheme 2) and its reduced analogue *N*-{2-[(pyridylmethyl)amino]phenyl}pyridine-2-carboxamide (H₂capcah, Scheme 2) are reported. These ligands were chosen because they have nitrogen donor atoms to mimic the environment of the copper in the oxidases, oxygenases and dioxygenases.



Scheme 2 The three ligands used for the synthesis of the copper(II) complexes.

The $Cu^{II}/Hcapcah^-$ and $Cu^{II}/capca^-$ compounds mimic the activity of the oxidases and oxygenases respectively inducing $2e^-$ oxidation of amine to imine and deamination of aromatic imine, by $4e^-$ oxidation of the imine nitrogen atom to an azinate group.

The copper(II) complex $2 \cdot CH_3OH$ constitutes the first example of a direct activation of dioxygen by a ligated to copper(II) $-HC=N-$ moiety as it was proven experimentally and theoretically. The mechanism of the oxidation of the ligated to copper(II) $-HC=N-$ functionality to an azinate group by means of a theoretical approach based on the Density Functional Theory (DFT) is also reported.

Experimental Materials.

All chemicals and solvents were purchased from Sigma-Aldrich and Merck, were of reagent grade and used without further purification, except pyridine-2-carboxaldehyde and 2-acetylpyridine which were distilled under high vacuum just prior to use. The condensation reaction of *N*-(2-aminophenyl)pyridine-2-carboxamide (Hpyca, see Scheme 3) with pyridine-2-carboxaldehyde or with 2-acetylpyridine was performed under high purity argon.

The mononuclear copper(II) compounds **1**·2H₂O-**3** were synthesized under high purity argon at ambient temperature ($\approx 20\text{ }^{\circ}\text{C}$), though compound **3** is stable in solution in air. C, H, and N analyses were conducted by the micro-analytical service of the School of Chemistry, the University of Glasgow. Copper was determined by atomic absorption and chloride gravimetrically as AgCl.

Merck silica gel 60 F₂₅₄ TLC plates were used for thin layer chromatography.

***N*-(2-Nitrophenyl)pyridine-2-carboxamide (Hpycan).** To a mixture of pyridine-2-carboxylic acid (71.48 g, 580.6 mmol) and 2-nitroaniline (80.12 g, 580.6 mmol) were added pyridine (25 mL) and triphenylphosphite (76.25 mL, 89.98 g, 290.3 mmol). The mixture was refluxed for 12 h under magnetic stirring. The resulting solution was refrigerated overnight at $-20\text{ }^{\circ}\text{C}$ yielding a brown-yellow precipitate. The solid was filtered off and washed with ethyl alcohol (2x50 mL), diethyl ether (2x 50 mL) and vacuum-dried. The yellow-brown solid was triturated with cold ($\approx 10\text{ }^{\circ}\text{C}$) ethyl alcohol (50 mL), filtered, and washed with diethyl ether (2 x 30 mL) and vacuum-dried to give 61.13 g of bright yellow solid. Yield, 43%. Mp $167\text{ }^{\circ}\text{C}$. Anal. Calcd for C₁₂H₉N₃O₃ ($M_r = 243.10$): C, 59.24; H, 3.73; N, 17.29. Found: C, 59.31; H, 3.76; N, 17.25. $R_f = 0.55$ (4:1 chloroform / *n*-hexane). [HR-ESI(+)-MS]: calcd for (C₁₂H₁₀N₃O₃Na) {[M+Na]}⁺ m/z 266.0536, found 266.0532 (100%).

***N*-{2-[(2-Pyridylmethylene)amino]phenyl}pyridine-2-carboxamide (Hcapca).** To a suspension of Hpycan(10.00 g, 41.14 mmol) and 1.50 g of hydrogenation catalyst (10% Pd on activated carbon) in acetone (350 mL), pure hydrogen was admitted for 24h under magnetic stirring. The mixture was filtered and the filtrate was evaporated to dryness to yield *N*-(2-aminophenyl)pyridine-2-carboxamide (Hpyca, Scheme 3) as a gold-yellow oil. The oil was redissolved in methyl alcohol (70 mL), 3.91 mL of pyridine-2-carboxaldehyde (4.410 g, 41.14 mmol) was added in one portion and the mixture was refluxed overnight under argon. The solution was cooled to -20°C for 5h and the resulting yellow-brown precipitate was filtered off, washed with diethyl ether (3x20mL) and vacuum-dried. The product was purified by Soxhlet extraction with *n*-hexane (200 mL) overnight. The volume of hexane was reduced to 50mL and was first cooled to room temperature ($\approx 20^\circ\text{C}$) and then to 0 °C for an hour. The resulting bright yellow precipitate was filtered off and washed with cold hexane (2 x 10 mL) and vacuum-dried to give 9.95g of product (80% based on Hpycan). Mp: 116-117 °C. Anal. Calcd for $\text{C}_{18}\text{H}_{14}\text{N}_4\text{O}$ ($M_r = 302.16$): C, 71.49; H, 4.67; N, 18.54. Found: C, 71.53; H, 4.67; N, 18.49. $R_f = 0.16$ (4:1 chloroform / *n*-hexane, v/v). [HR-ESI(+)-MS]: calcd for $(\text{C}_{18}\text{H}_{15}\text{N}_4\text{ONa})\{[\text{M}+\text{Na}]\}^+$ m/z 325.1060, found 325.1056 (100%).

***N*-{2-[(Pyridylmethyl)amino]phenyl}pyridine-2-carboxamide (H₂capcah).** The organic molecule was synthesized according to literature⁶³ and its purity was checked with positive HR-ESI-MS, ¹H-, ¹³C-NMR spectra and elemental analysis. Anal. Calcd for $\text{C}_{18}\text{H}_{16}\text{N}_4\text{O}$ ($M_r = 304.18$): C, 71.02; H, 5.30; N, 18.41. Found: C, 71.05; H, 5.31; N, 18.39. Mp: 104-105°C. $R_f = 0.07$ (4:1 chloroform/*n*-hexane, v/v). [HR-ESI(+)-MS]: calcd for $(\text{C}_{18}\text{H}_{16}\text{N}_4\text{ONa})\{[\text{M}+\text{Na}]\}^+$ m/z 327.1216, found 327.1212 (100%).

***N*-{2-[1-(pyridine-2-yl)ethylideneamino]phenyl}picolinamide (Hmcapca).** The ligand Hmcapca was prepared in a similar fashion to Hcapca except that 2-

acetylpyridine was used instead of pyridine-2-carboxaldehyde in yield 50%. Melting point: 94-95 °C. Anal. Calcd for C₁₈H₁₄N₄O (*M_r* = 316.15): C, 72.13; H, 5.10; N, 17.71. Found: C, 72.03; H, 5.05; N, 17.65. *R_f* = 0.12 (4:1 chloroform / n-hexane, v/v). [HR-ESI(+)-MS]: calcd for (C₁₈H₁₄N₄ONa) {[M+Na]⁺} *m/z* 339.1216, found 339.1211 (100%).

***N*-{2-[(Pyridylmethyl)amino]phenyl}pyridine-2-carboxamido-(*N_{py}*, *N_{am}*, *N_{im}*, *N_{py}*)}chloridocopper(II), [Cu^{II}(Hcapcah)Cl]·2H₂O (1·2H₂O).** CuCl₂·2H₂O (0.112 g, 0.657 mmol) was dissolved under argon in methyl alcohol (5 mL) and then, solid H₂capcah (0.200 g, 0.657 mmol) was added in one portion to the stirred solution. Upon addition of the ligand the blue color of the solution turned to green and a green precipitate was formed. The mixture was stirred for three hours and then, it was filtered off, washed with cold methyl alcohol (2 x 3 mL) and diethyl ether (2 x 5 mL) and vacuum-dried to give 0.275 g of a green solid. Yield, 95% (based on CuCl₂·2H₂O). Anal. Calcd for 1·2H₂O, [C₁₈H₁₉ClCuN₄O₃ (*M_r* = 438.19)]: C, 49.30; H, 4.37; Cl, 8.09; Cu, 14.50; N, 12.79. Found: C, 49.26; H, 4.38; Cl, 8.18; Cu, 14.67; N, 12.77. [HR-ESI(+)-MS]: calcd for C₁₈H₁₅N₄OCu {[M-Cl-2H₂O]⁺} *m/z* 366.0536, found 366.0531 (100%).

Green crystals of **1** suitable for X-ray diffraction analysis were obtained by layering a methyl alcohol solution of H₂capcah into a methyl alcohol solution of CuCl₂·2H₂O.

{*N*-[2-((2-Pyridylmethylene)amino)phenyl]pyridine-2-carboxamido-(*N_{py}*, *N_{am}*, *N_{im}*, *N_{py}*)}chloridocopper(II), [Cu^{II}(capca)Cl]·CH₃OH (2·CH₃OH). The compound **2**·CH₃OH was prepared (in 88% yield) in the same way as compound **1**·2H₂O except that Hcapca was used instead of H₂capcah. The color of the compound **2**·2H₂O is brick red. Yield: Anal. Calcd for 2·CH₃OH, [C₁₉H₁₇ClCuN₄O₂ (*M_r* = 432.18)]: C, 52.76; H, 3.96; Cl, 8.20; Cu, 14.70; N, 12.96. Found: C, 52.66; H, 3.89; Cl, 8.18; Cu,

14.67; N, 12.88. [HR-ESI(+)-MS]: calcd for $C_{18}H_{13}CuN_4O$ $\{[M-Cl-CH_3OH)]^+\}$ m/z 364.0380, found 364.0374 (100%).

Crystals of **2**·CH₃OH suitable for X-ray diffraction analysis were obtained by layering a methyl alcohol solution of Hcapca into a methyl alcohol solution of CuCl₂·2H₂O.

{N-(2-(1-(pyridine-2-yl)ethylideneamino)phenyl)picolinamido-(N_{pyr}, N_{am}, N_{im}, N_{pyr})}chloridocopper(II), [Cu^{II}(mcapca)Cl] (3). Complex **3** was prepared in a similar way to complex **2**·CH₃OH except that Hmcapca was used instead of Hcapca. Yield: 91% (based on CuCl₂·2H₂O). Anal. Calcd for, [C₁₉H₁₇ClCuN₄O₂ (M_r = 432.16)]: C, 52.70; H, 3.96; Cl, 8.20; Cu, 14.70; N, 12.96. Found: C, 52.67; H, 3.84; Cl, 8.18; Cu, 14.67; N, 13.18. [HR-ESI(+)-MS]: calcd for (C₁₉H₁₅CuN₄O) $\{[M-Cl]^+\}$ m/z , 378.0536 found 378.0532 (100%).

Crystals of **3** suitable for X-ray diffraction analysis were obtained by layering diethyl ether into a concentrated methyl alcohol solution of **3**.

μ-Bis-[(Z)-[(E)-2-(2-(picolinamido)phenylimino)-2-(pyridin-2-yl)ethylidene]azinate}dicopper(II), [Cu^{II}₂(μ-η¹, η¹-pipyaz-O,O')₂], (4).

Method A. Compound **1**·2H₂OH or **2**·CH₃OH was dissolved in CH₃OH (≈ 4 mg/ml) at ambient temperature (30 °C). The solution magnetically stirred for 5 hours in air and then, diethyl ether was layered on it to get just a few yellow-brown crystals of **4** suitable for X-ray diffraction analysis.

Method B. Compound **4**, as yellow-brown crystals, was prepared in yield 10% using the same method for the preparation of **2**·CH₃OH except that i) [Cu^{II}(CH₃COO)₂]·H₂O was substituted for CuCl₂·2H₂O, ii) the experiment was conducted in air at ambient temperature (30 °C) for 4 hours and iii) the solution was layered with diethyl ether.

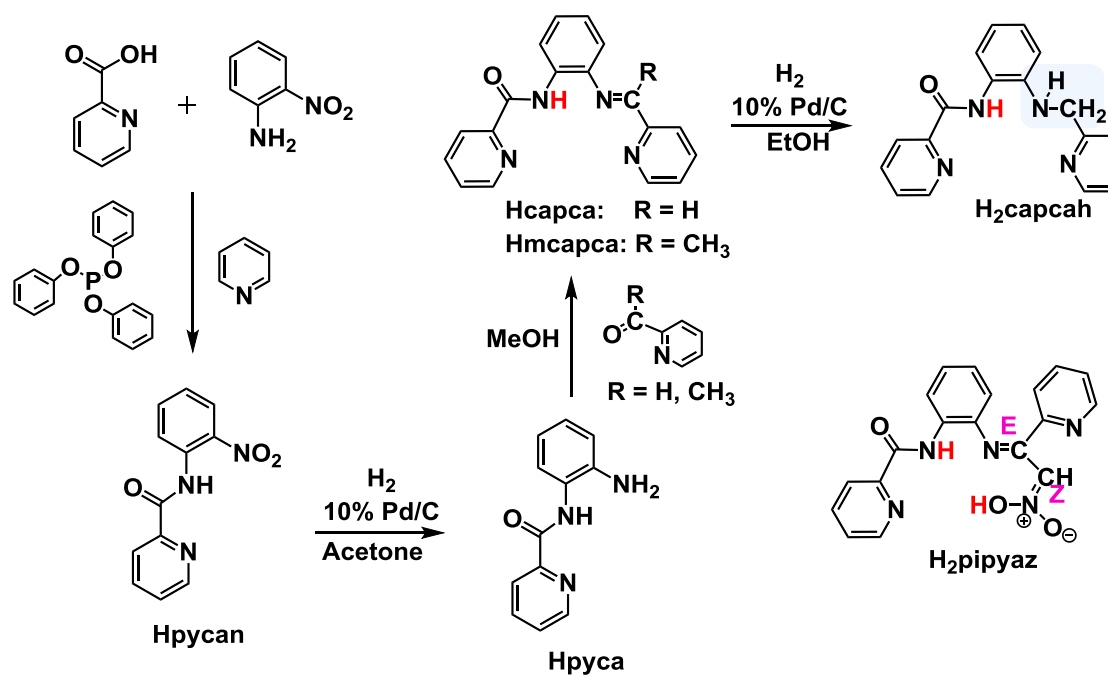
Anal. Calcd for $[C_{38}H_{26}Cu_2N_{10}O_6]$ ($M_r = 845.40$): C, 53.81; H, 3.09; Cu, 14.99; N, 16.52. Found: C, 53.90; H, 3.13; Cu, 14.97; N, 16.44.

Results and discussion

Synthesis of the ligands and copper(II) compounds

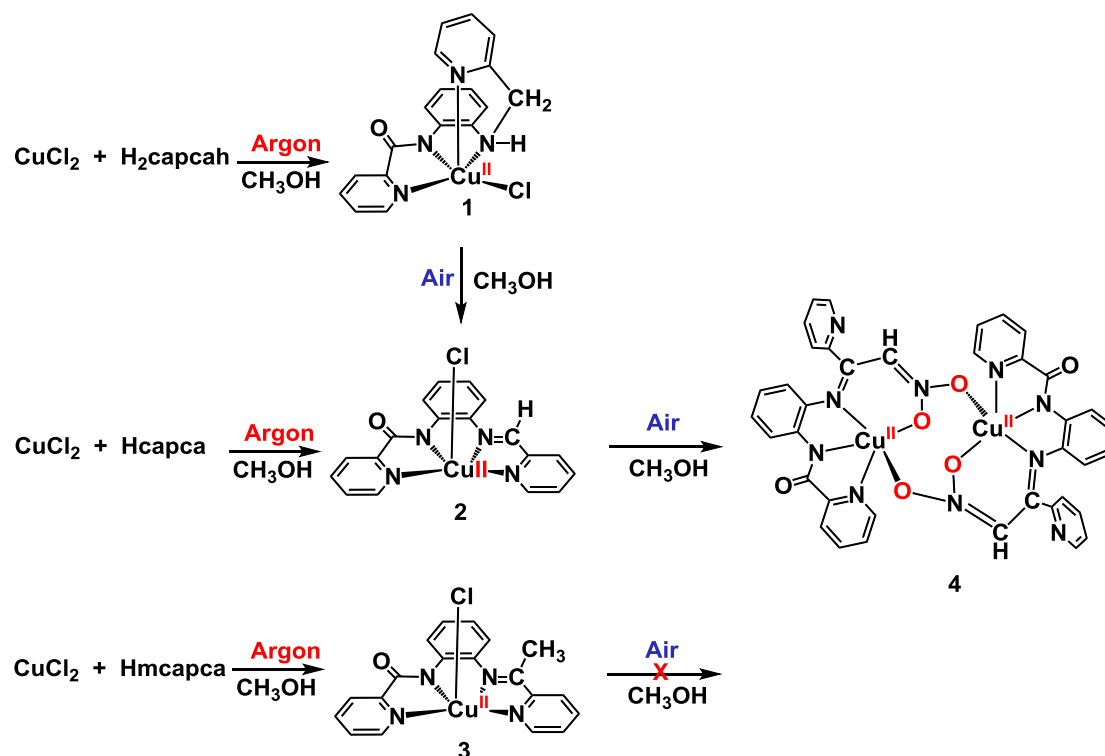
The synthesis of the three ligands, i. e., Hcapca, its reduced and methylated analogues H₂capcah and Hmcapca respectively used in this study for the synthesis of the copper(II) compounds, and the structure of the azinate molecule H₂pipyz, formed as its copper(II) complex from the interaction of the species $[Cu^{II}(capca)]^+$ with dioxygen (vide infra), are depicted in Scheme 3.

The organic molecules Hpycan and Hcapca (Scheme 3) were synthesized by modifications of reported procedures^{64, 65} to obtain better product yields, and to avoid the isolation of Hpyca (Scheme 3), while the organic molecule H₂capcah was prepared according to literature.⁶³ The completion of the reductions of Hpycan to Hpyca (-NO₂ to -NH₂) and of Hcapca to H₂capcah (-N=CH- to -NH-CH₂-) was followed by TLC. The molecule Hpyca was not isolated, but it was condensed with pyridine-2-carboxaldehyde or 2-acetylpyridine under high purity argon to avoid the oxidation of the amine group. Soxhlet extraction of the crude Hcapca or Hmcapca proved quite effective purification method.



Scheme 3 The synthesis of the three ligands used in this study and the structural formula of the ligand H₂piyaz.

The synthesis of the copper(II) compounds with the ligands H₂capcah, Hcapca and Hmcapca is depicted in Scheme 4. The methyl alcohol solutions of the mononuclear copper(II) compounds, **1**·2H₂O and **2**·CH₃OH, are oxidized by air to complex **4**, while the methyl alcohol solution of the copper(II) compound **3** remains stable in air.



Scheme 4 The synthesis of the copper(II) complexes **1**, **2**, **3**, and **4**.

X-ray crystallographic results

A summary of the crystallographic data and the final refinement details for compounds **1–4** are given in Table S1. Interatomic distances and bond angles relevant to the copper(II) coordination sphere are listed in Table 1. Fig. 1A shows a perspective view of compound **1**. In **1** the copper (II) atom is bonded to the two pyridine [N(1) and N(4)], the deprotonated amide N(2), and the secondary amine N(3) nitrogen atoms of the singly deprotonated ligand Hcapcah^- and one chloride ion. The coordination geometry for the Cu^{II} center is best described as a distorted square pyramidal; the distortion parameter τ ,⁶⁶ is calculated to be 0.090. The copper(II) atom is displaced from the N_3Cl coordination plane [root mean square (rms) 0.149 Å] by 0.254(2) Å towards the pyridine nitrogen atom N(4), which occupies the apical position. Of the four $\text{Cu}^{\text{II}}\text{-N}$ bonds, the bond length to N(2) [$d(\text{Cu}^{\text{II}}\text{-N}_{\text{amide}}) = 1.942(2)$

Å], that is, the deprotonated amide nitrogen, is consistent with the literature values.⁶⁷⁻
⁶⁹The bond length to N(3) [2.046(2) Å], the secondary amine nitrogen, is substantially longer (about 0.1 Å) than the Cu^{II}-N_{imine} bond length [1.942(3) Å] of compound **2**·CH₃OH (vide infra). The bond lengths to N(1) [1.994(2) Å] and N(4) [2.273(1) Å], the pyridine nitrogens, are longer than the Cu^{II}-N_{amide} bond length and different from each other as a consequence of the difference in their positions: basal plane for [N(1)], versus apex for [N(4)] of the square pyramid.

The crystal structure of **2**·CH₃OH is shown in Fig. 1B. A notable difference between the X-ray crystal structure of **1** and **2**·CH₃OH is the almost planar conformation of the ligand capca⁻ in the latter as opposed to non-planar conformation of ligand Hcapca⁻ in **1**, due to sp³ hybridization of C(13) (Fig. 1A). The coordination geometry for the Cu^{II} center in **2**·CH₃OH is best described as a slightly distorted square pyramidal; the distortion parameter τ ,⁶⁶ is calculated to be 0.048. The copper(II) ion is displaced from the N₄ basal plane [root mean square (rms) 0.025 Å] by 0.261 Å towards the Cl(1) which is the apex of the square pyramid. The chloride provides the longest bond to the copper(II) ion, 2.527(1) Å, and the two pyridine nitrogen bond distances [2.041(3) and 2.060(4) Å] are longer than the amide [1.939(4) Å] and imine [1.942(3) Å] ones. The almost identical Cu^{II}-N_{amide} and Cu^{II}-N_{imine} bond lengths in compound **2**·CH₃OH imply a considerable delocalization of π -electron density in the skeleton of the ligand capca⁻. The Cu^{II}-N_{amide} and Cu^{II}-N_{pyridine} bond lengths are in the expected range.⁶⁷⁻⁶⁹

Table 1 Interatomic distances (Å) and angles (deg) relevant to the copper(II) coordination sphere.

parameter	1	2 ·CH ₃ OH	3	4
Cu(1) - X ^a	2.2684(6)	2.527(1)	2.473(1)	2.685(2)

Cu(1) - N(1)	1.994(2)	2.041(3)	2.015(2)	1.989(2)
Cu(1) - N(2)	1.942(2)	1.939(4)	1.942(2)	1.891(3)
Cu(1) - N(3)	2.046(2)	1.942(3)	1.982(2)	1.945(2)
Cu(1) - N(4)	2.273(1)	2.060(4)	2.039(2)	1.897(2)
X - Cu(1) - N(1)	98.68(5)	94.9(1)	96.9(7)	93.33(7)
X - Cu(1) - N(2)	160.09(5)	102.7(1)	104.5(6)	94.01(9)
X - Cu(1) - N(3)	94.21(5)	99.7(1)	104.2(7)	92.57(8)
X - Cu(1) - N(4)	99.16(4)	94.5(1)	95.8(6)	86.48(7)
N(1) - Cu(1) - N(2)	82.18(6)	82.1(1)	81.9(8)	83.6(1)
N(1) - Cu(1) - N(3)	165.48(6)	160.5(1)	155.8(8)	167.72(9)
N(1) - Cu(1) - N(4)	105.96(6)	110.9(1)	109.6(8)	94.36(8)
N(2) - Cu(1) - N(3)	83.43(6)	82.0(2)	81.3(8)	85.2(1)
N(2) - Cu(1) - N(4)	99.70(6)	157.6(1)	155.4(8)	178.0(1)
N(3) - Cu(1) - N(4)	78.35(6)	81.0(1)	80.4(7)	96.75(9)

^aX corresponds to Cl(1) and O(3) for compounds **1**, **2**·CH₃OH, **3** and **4** respectively.

It is worth noting that the large difference in Cu^{II}-Cl bond lengths, 2.2684(6) Å vs 2.527(1) Å in compounds **1** and **2**·CH₃OH respectively, is nicely reflected in the Far-IR spectra of them with $\nu(\text{Cu-Cl})$ at 359 (**1**) and 268 cm⁻¹ (**2**·CH₃OH). Compound **3** with a $d(\text{Cu}^{\text{II}}\text{-Cl}) = 2.473(1)$ Å gave a $\nu(\text{Cu-Cl})$ at 306 cm⁻¹. Details for the IR spectra of all the copper(II) compounds are presented in the SI (pages S5, S6 and Table S2).

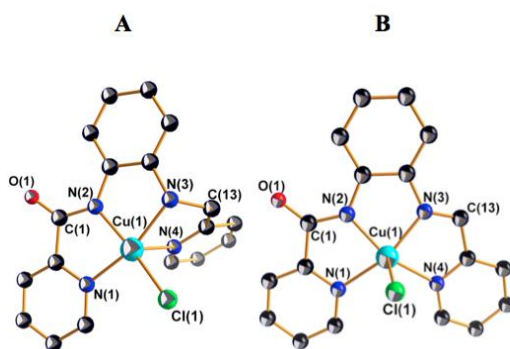


Fig. 1 Structural representation of **1** (A) and **2**·CH₃OH (B) with thermal ellipsoids drawn at 50% probability level. Hydrogen atoms and solvent molecules are omitted for clarity.

The structural features of complex **3** (Fig. 2) are very similar with those of **2**·CH₃OH and thus, this structure will not be further discussed.

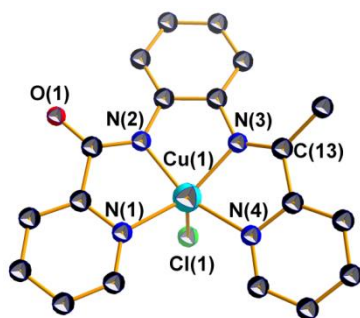
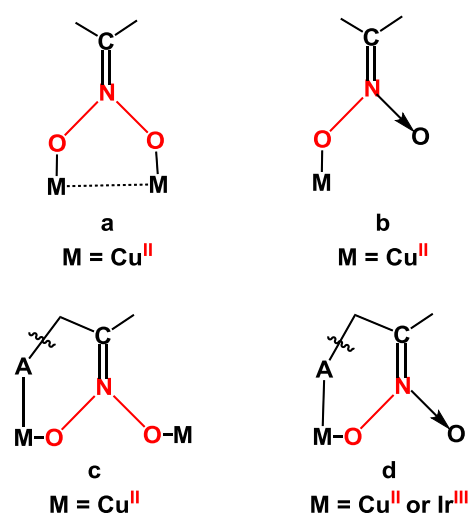


Fig. 2 Structural representation of compound **3** (thermal ellipsoids represent 50% probability). Hydrogen atoms are omitted for clarity.

The molecular structure of the compound [Cu^{II}₂(μ-η¹-η¹-pipyaz-*O,O'*)₂] (Fig. 3) is a centrosymmetric dimer formed by two bridging azinate-*O,O'*-ligands. It represents the first structurally characterized copper(II) complex, and in general of any transition metal complex, that contains a bridging η¹-η¹ azinate-*O,O'* coordination mode, where the azinate group is part of a chelate ring (Scheme 5c). The coordination modes **5a** and **5b** for azinates have been observed for copper(II)⁷⁰ and the mode **5d** for

copper(II)⁷¹ and iridium(III)⁷² compounds. In $[\text{Cu}^{\text{II}}_2(\mu\text{-}\eta^1\text{-}\eta^1\text{-pipyaz-}O,O')_2]$ each copper(II) atom is coordinated by the three nitrogen atoms [i.e., the pyridine [N(1)], the deprotonated amide N(2), and the imine N(3) nitrogen] provided by the same doubly deprotonated pipyaz²⁻ ligand and by two oxygen atoms O(2) and O(3)' from the two azinate moieties one of them provided by the symmetry-related unit, while the pyridine nitrogen [N(4)] and its symmetry related [N(4)]' atoms remain uncoordinated. The two oxygen donor atoms bridge the two copper(II) atoms in the complex, keeping them 5.118 Å apart. The configuration of the pipyaz²⁻ ligand with respect to the N(3) = C(13) and C(19) = N(5) bonds is *E*, and *Z* respectively.



Scheme 5 The bonding modes (**a**, **b** and **d**) of the azinate group observed in transition metal complexes and the new bonding mode (**c**) present in $[\text{Cu}^{\text{II}}_2(\mu\text{-}\eta^1,\eta^2\text{-pipyaz-}O,O')_2]$ (**4**).

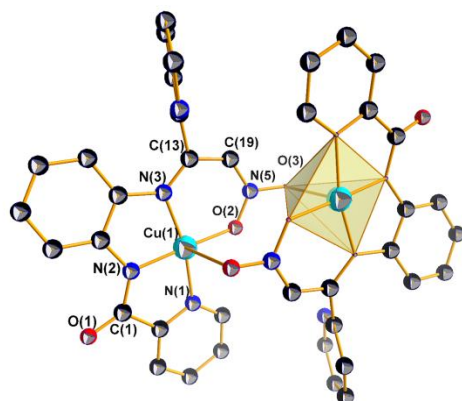


Fig. 3 Structural representation of the centrosymmetric dinuclear compound $[\text{Cu}^{\text{II}}_2(\mu\text{-}\eta^1\text{-}\eta^1\text{-pipyaz-}O,O')_2]$ (**4**) with thermal ellipsoids at 50% probability. Hydrogen atoms are omitted for clarity.

The coordination sphere around each copper(II) atom in $[\text{Cu}^{\text{II}}_2(\mu\text{-}\eta^1\text{-}\eta^1\text{-pipyaz-}O,O')_2]$ can be described as a distorted square pyramidal; the distortion parameter τ ,⁶⁶ is calculated to be 0.171. The oxygen O(3)' occupies the apex at a distance of 2.685 Å, while, the three nitrogen atoms and the azinate oxygen atom O(2) of the bridging ligand pipyaz^{2-} constitute the basal plane around Cu(II). The root mean squared (r.m.s.) deviation of the four basally coordinated atoms of Cu(1) from the mean plane is 0.217 Å, with the metal atom placed at 0.071(1) Å away from the plane, toward the O(3)' atom.

It is worth noting that the two azinate units in the dinuclear compound $[\text{Cu}^{\text{II}}_2(\mu\text{-}\eta^1\text{-}\eta^1\text{-pipyaz-}O,O')_2]$ form with the two copper atoms an eight-membered ring (Fig. 3).

UV-vis spectroscopy

The UV-vis spectral data of the compounds **1**·2H₂O-**4** are listed in Table 2. The peaks of all complexes were assigned to intraligand and charge transfer transitions. In addition to these peaks **1**·2H₂O gave one peak at 675 nm, which was assigned to a *d-d*

transition. The oxidation of compounds **1**·2H₂O and **2**·CH₃OH in CH₃OH by air was followed with UV-vis spectroscopy. In Fig. 4A, it is shown the variation of the absorbance in the UV-vis spectrum of the compound **1**·2H₂O (0.16 mM) in CH₃OH with time. The initial rates of the oxidation of complexes **1**·2H₂O and **2**·CH₃OH by air dioxygen are linearly dependent on their concentrations (Fig. 4B). The rate constants of the oxidation reactions, were calculated from the slopes of the lines (Fig. 4B), and were: $0.013 \pm 0.001 \text{ min}^{-1}$, $0.10 \pm 0.01 \text{ min}^{-1}$, and $2.3 \pm 0.1 \text{ min}^{-1}$ for **1**·2H₂O, **2**·CH₃OH, and **2**·CH₃OH with one equivalent of Et₃N respectively. The smaller rate of oxidation of **1**·2H₂O in comparison to **2**·CH₃OH reflects the additional oxidation step required for **1**·2H₂O (**1**·2H₂O is oxidized first to **2**·CH₃OH). The addition of the base increases dramatically the reaction rate, and this is in agreement with the proposed proton released mechanism of the formation of compound **4** (vide infra).

Table 2 UV-vis spectral data for the copper(II) compounds **1**·2H₂O-**4**

Compound	Solvent	λ_{max} [nm] (ϵ [M ⁻¹ cm ⁻¹])
1 ·2H ₂ O	acetonitrile	675 (100), 336 (4 600)
2 ·CH ₃ OH	acetonitrile	449 (1500), 332 (5 000)
3	methanol	274 (17 500), 325 sh (8 000)
4	methanol	647 (600), 448 (8 700), 327 (26 000), 292 (14 500)

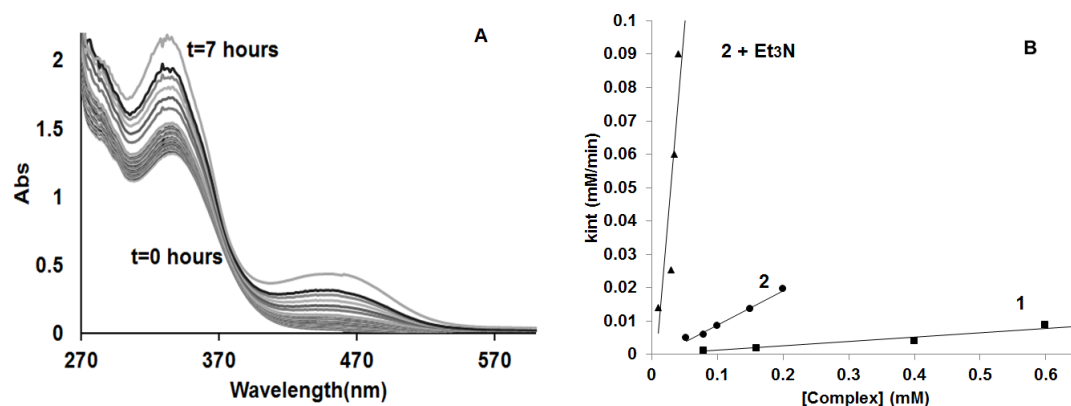


Fig. 4 A) Variation of the absorbance in the UV-vis spectrum of the compound **1**·2H₂O (0.16 mM) in CH₃OH with time. B) Diagram of the initial oxidation rates of the copper(II) complexes **1**·2H₂O, **2**·CH₃OH, and **2**·CH₃OH with one equivalent Et₃N in methyl alcohol in relation to their concentration.

The UV-vis spectral changes of compounds **2**·CH₃OH (0.080 mM) and **3** (0.080 mM) in CH₃OH with time (0 to 30 min) are shown in Fig. 5. The spectrum of **3**, up to 24 hours, does not show any change, suggesting that the oxidation rate of **3** by air dioxygen, is much slower in comparison to **2**.

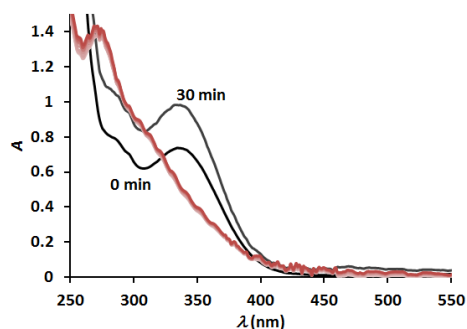


Fig. 5 Variation of the absorbance in the UV-vis spectra of the compounds **2**·CH₃OH (black line) and **3** (red line) in CH₃OH with time.

EPR spectroscopy

The X-band c. w. EPR spectra of frozen methyl alcohol solutions of complexes **1**·2H₂O, and **2**·CH₃OH gave an unresolved broad peak for each complex, at $g=2.048$

and 2.191 respectively. The X-band c. w. EPR spectrum of a frozen methyl alcohol solution of **3** gave a rhombic anisotropic spectrum exhibiting a superhyperfine splitting with the four equatorial nitrogen atoms (Fig. 6). The simulated spectrum was best fitted using the following parameters: $g_z=2.211$, $g_y=2.063$, $g_x=2.034$ and $A_z=182$, $A_y=12$, $A_x=12$, $A_{zN1}=8$, $A_{yN1}=7$, $A_{xN1}=11$, $A_{zN2}=11$, $A_{yN2}=11$, $A_{xN2}=17$, $A_{zN3}=13$, $A_{yN3}=12$, $A_{xN3}=8$, $A_{zN4}=12$, $A_{yN4}=11$, $A_{xN4}=16 \times 10^{-4} \text{cm}^{-1}$. The parameters are consistent with a $\text{Cu}^{\text{II}}\text{-N}_4$ system.⁷³

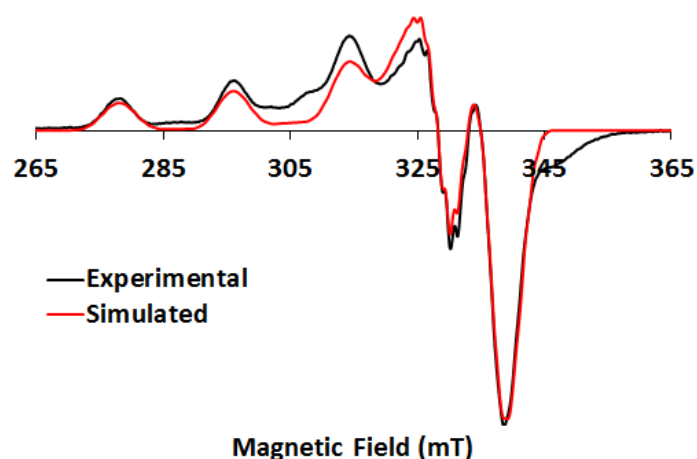


Fig. 6 X-band c. w. EPR spectrum of **3** (0.16 mM) in frozen MeOH (black line) and its simulated one (red line).

The X-band c. w. EPR spectrum of complex **4** in frozen CH_3OH gave also a rhombic anisotropic spectrum exhibiting a superhyperfine splitting with the three equatorial nitrogen atoms (Fig. 7) and its simulated spectrum was best fitted using the following parameters: $g_z=2.213$, $g_y=2.067$, $g_x=2.035$ and $A_z=186$, $A_y=11$, $A_x=11$, $A_{zN1}=7$, $A_{yN1}=12$, $A_{xN1}=14$, $A_{zN2}=16$, $A_{yN2}=10$, $A_{xN2}=12$, $A_{zN3}=10$, $A_{yN3}=15$, $A_{xN3}=5 \times 10^{-4} \text{cm}^{-1}$.¹ The parameters are consistent with a $\text{Cu}^{\text{II}}\text{-N}_3\text{O}$ system.⁷³

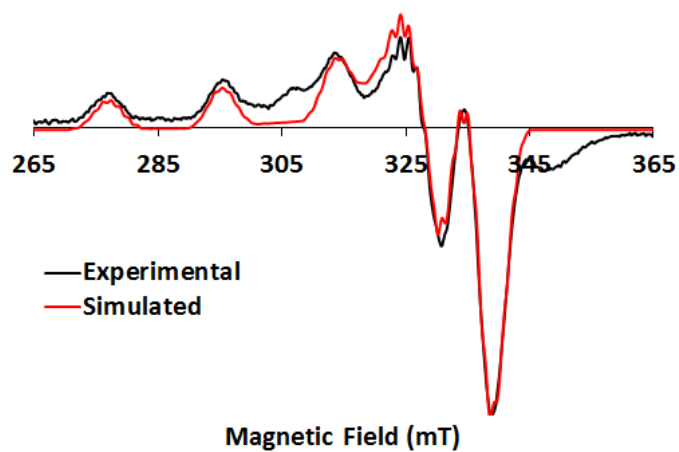


Fig. 7 The X-band c. w. EPR spectrum of compound **4** (0.16 mM) in frozen MeOH (black line) and its simulated one (red line).

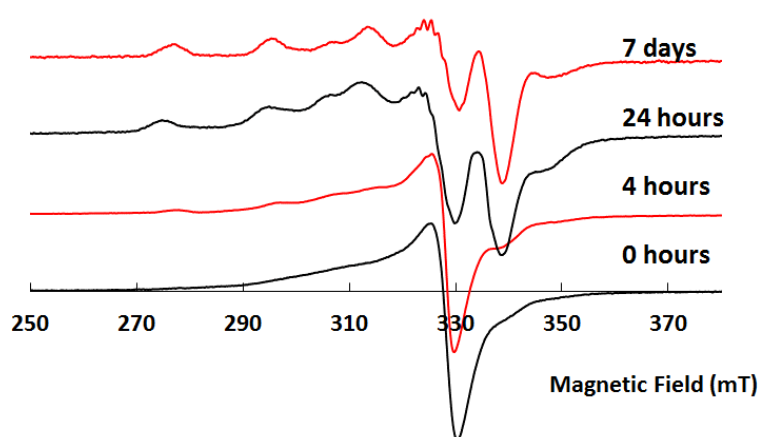


Fig. 8 The X-band c. w. EPR spectrum of $2\cdot\text{CH}_3\text{OH}$ in frozen CH_3OH (0.80 mM) with time.

The oxidation of $1\cdot 2\text{H}_2\text{O}$ and $2\cdot\text{CH}_3\text{OH}$ to **4** in CH_3OH by air was also monitored by X-band c. w. EPR spectroscopy. In Fig. 8, they are shown the X-band c. w. EPR

spectra of **2**·CH₃OH as a function of the time. In addition to the peaks of compound **4** a broad (~20 gauss) peak at $g=1.941$ was formed. This value is very low for a Cu^{II}centered radical and thus, it was assigned to an organic centered radical.⁷⁴ The formation of the organic radical is justified by the first step of the mechanism of oxidation of [Cu^{II}(capca)]⁺ to the azinate complex (Fig. 13) proposed by the theory, in which the O₂ binds to the carbon atom of the imine group of [Cu^{II}(capca)]⁺(Fig. 11) transforming dioxygen to a superoxy radical. The X-band c. w. EPR spectrum of **3** in CH₃OH does not show any change after the exposure of the solution to air for 24 h.

ESI-MS spectroscopy

The oxidation of [Cu^{II}(Hcapcah)]⁺ (**1'**) to [Cu^{II}(capca)]⁺ (**2'**) in CH₃OH solution was monitored by ESI-MS in real time and it takes approximately 24 h, however in the presence of one equivalent of Et₃N the reaction proceeds to completion almost instantly in agreement with UV-vis studies. Concurrently with the distribution envelopes of the species [Cu^{II}(Hcapcah)]⁺ and [Cu^{II}(capca)]⁺ centred at $m/z = 364.03$ and 366.05 respectively, an additional envelope centred at $m/z=786.09$ was observed which can be assigned to {[Cu^{II}(pipyaz)][Cu^{II}(capca)]⁺} which became dominant after 24 h (Fig. S1). This is in agreement with the results found from UV-vis kinetic studies, whereas the oxidation of [Cu^{II}(capca)]⁺ to [Cu^{II}(pipyaz)] is faster than the oxidation of [Cu^{II}(Hcapcah)]⁺ to [Cu^{II}(capca)]⁺.

In addition, MS studies were conducted in solutions containing one equivalent [Cu^{II}(CH₃COO)₂]·H₂O and one or two equivalents of Hcapca immediately and 6 hours after mixing the solutions. The recorded spectra revealed a major distribution envelope centered at 364.03 which can be assigned to [Cu^{II}(capca)]⁺. The additional distribution envelope centered at 286.11 was assigned to the [Hcapca(-H₂O)+H⁺]

species, whereas minor envelopes centered at 303.20 and 325.12 can be assigned to the $[\text{Hcapca}+\text{H}^+]$ and $[\text{Hcapca}+\text{Na}^+]$ respectively. The 1:2 solutions revealed additionally an envelope assigned to $\{[\text{Cu}(\text{capca})]^++\text{Hcapca}\}$ ($m/z = 666.25$) adduct. The envelope observed at $m/z 786.09$ can be assigned to $\{[\text{Cu}^{\text{II}}(\text{pipyaz})][\text{Cu}^{\text{II}}(\text{capca})]^+\}$ species. This peak is present in both $\text{Cu}^{\text{II}}(\text{CH}_3\text{COO})_2$ -Hcapca mixtures and becomes dominant in the region 300-900 m/z values after 6 hours. The envelopes originated from $[\text{Cu}^{\text{II}}(\text{capca})]^+$ -Hcapca adducts as well the Hcapca ionized and dehydrated species are reduced as a function of the time, while the amount of Hcapca present in the reaction mixture is consumed.

Finally, MS studies were conducted in CH_3OH solutions containing one equivalent of $\text{Cu}^{\text{II}}\text{Cl}_2\cdot\text{H}_2\text{O}$ and one equivalent of Hmcapca immediately, 6 hours and 24 hours after mixing the solutions (Fig. 9). The recorded spectra revealed a major distribution envelope centered at 378.06 which can be assigned to $[\text{Cu}^{\text{II}}(\text{mcapca})]^+$ with traces of $[(\text{Cu}^{\text{II}} \text{mcapca})_2\text{Cl}]^+$ (798.08) (Fig. 9) and some tiny peaks of unreacted material. After 6hrs the only difference is that the unreacted material is almost gone and the peak which corresponds to two individual clusters “flying” together becomes more intense (Fig. 9). Finally, after 24hrs the unreacted material has completely disappeared, and the two remaining distribution envelopes attributed to the complex is the only species that we can detect (Fig. 9).

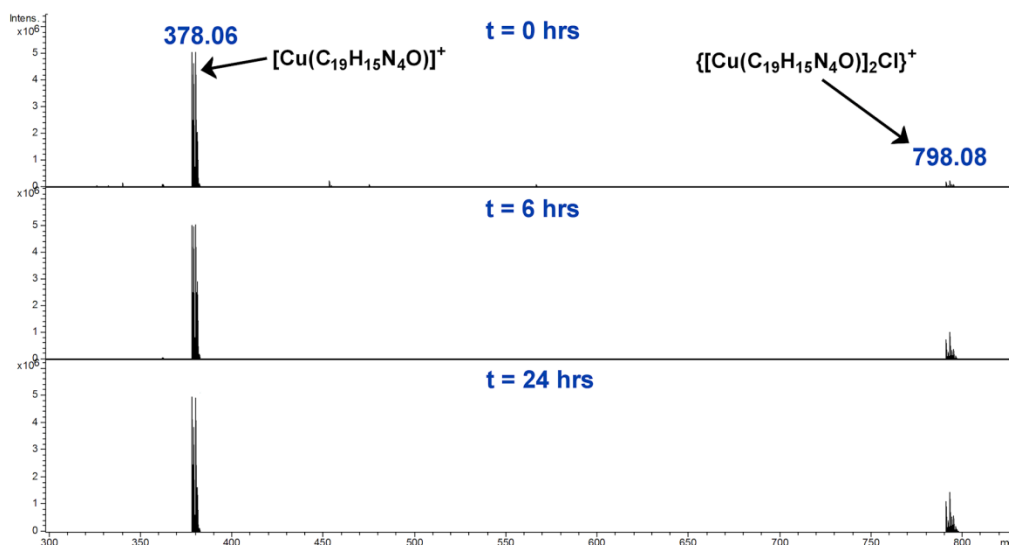


Fig. 9 ESI-MS of the system $\text{Cu}^{\text{II}}\text{Cl}_2\cdot\text{H}_2\text{O}/\text{Hmcapca}$ (1:1 molar ratio) in methyl alcohol at 0, 6 and 24 hours after mixing $\text{Cu}^{\text{II}}\text{Cl}_2\cdot\text{H}_2\text{O}$ and Hmcapca.

Theoretical studies

First we calculated the potential energy surface (PES) for the transformation of the amine-Cu(II) complex, $[\text{Cu}^{\text{II}}(\text{Hcapcah})]^+$ (**1'**) to imine-Cu(II) complex, $[\text{Cu}^{\text{II}}(\text{capca})]^+$ (**2'**) by air oxidation. The geometric and energetic reaction profile for the **1'** \rightarrow **2'** transformation by air oxidation, calculated at the PBE0/Def2-TZVP level of theory in methyl alcohol solution is depicted schematically in Fig. 10.

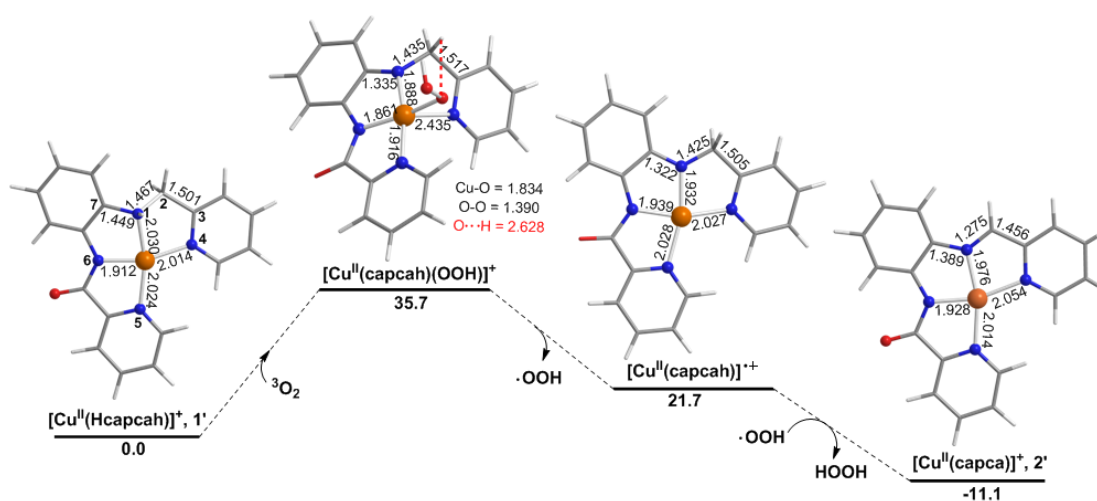


Fig. 10 Geometric and energetic reaction profile for the **1'** \rightarrow **2'** transformation by air oxidation, calculated at the PBE0/Def2-TZVP level of theory in methyl alcohol solution.

The first step of the reaction pathway of the oxidation of **1'** to **2'** involves the activation of dioxygen by interaction with it. Calculations located on the PES revealed a local minimum corresponding to a $[\text{Cu}^{\text{II}}(\text{Hcapcah})(\text{OOH})]^+$ association involving coordination of a hydroperoxyl group to Cu(II) metal center resulted through a homolytic amine H atom abstraction by dioxygen. The estimated O-O bond distance of 1.390 Å and the harmonic vibrational stretching frequency, $\nu_{\text{O-O}}$, of 988 cm^{-1} characterize the hydroperoxyl nature of the coordinated $\bullet\text{OOH}$ radical.

The $[\text{Cu}^{\text{II}}(\text{Hcapcah})(\text{OOH})]^+$ intermediate is a transient species, since immediately releases the $\bullet\text{OOH}$ radical yielding the $[\text{Cu}^{\text{II}}(\text{capcah}\bullet)]^+$ ($S = 1$) intermediate, which abstracts a methylenic H atom to produce the imine-Cu(II) species **2'**. The release of the $\bullet\text{OOH}$ radical followed by the methylenic H atom abstraction corresponds to an exothermic process ($\Delta H = -46.8$ kcal/mol). Alternatively the coordinated $\bullet\text{OOH}$ radical could attack and abstract the methylenic H atom, which is found 2.628 Å far from the coordinated O donor atom of $\bullet\text{OOH}$, yielding the imine-Cu(II) species **2'**.

To understand why the copper(II) atom in the complex **1'** coordinates the dioxygen reduced species ($\bullet\text{OOH}$) and does not coordinate the molecular O_2 we looked at the Frontier Molecular Orbitals (FMOs) and the natural atomic charge distribution of the complexes and the possible transient intermediate (Fig. S2).

Inspection of Fig. S2 reveals that the Singly Occupied Molecular Orbital (SOMO) and the Lowest Unoccupied Molecular Orbital (LUMO) of $[\text{Cu}^{\text{II}}(\text{Hcapcah})]^+$ are mainly localized on the aromatic phenyl moieties of the $[\text{Cu}^{\text{II}}(\text{Hcapcah})]^+$ species. The SOMO involves only very small components located on the amine N (0.55%) and H (0.36%) atoms as well as on the methylenic C atom (0.12%). Therefore, the interaction of the Highest Occupied Molecular Orbital (HOMO) of triplet dioxygen

(π_{1g}^* MO) with the SOMO and LUMO of $[\text{Cu}^{\text{II}}(\text{Hcapcah})]^+$ is not possible to drive the coordination of dioxygen to Cu(II) forming a $[\text{Cu}(\text{Hcapcah})(\text{O}_2)]^+$ adduct. In effect dioxygen abstracting the amine H atom from the Hcapcah⁻ ligand is converted to a hydroperoxyl ($\bullet\text{OOH}$) radical which could be coordinated to the Cu(II) metal center yielding the transient $[\text{Cu}^{\text{II}}(\text{capcah})(\bullet\text{OOH})]^+$ intermediate. The natural atomic charges on the coordinated O donor atom of OOH ($q_{\text{O}} = -0.342$ |e|) and the methylenic H atom ($q_{\text{H}} = 0.255$ |e|) in the transient $[\text{Cu}^{\text{II}}(\text{capcah})(\bullet\text{OOH})]^+$ intermediate support electrostatic interactions which are responsible for the $\bullet\text{H}$ atom abstraction and formation of hydrogen peroxide, H_2O_2 .⁷⁵

Next we calculated the potential energy surface (PES) for the transformation of the imine-Cu(II) complex **2'** to azinate-Cu(II), $[\text{Cu}^{\text{II}}(\text{pipyz})]$ complex by air oxidation. As it is the case for the $[\text{Cu}^{\text{II}}(\text{Hcapcah})]^+$ (**1'**) complex, coordination of dioxygen to Cu^{II} metal center in either in an end-on or a side-on coordination mode was not possible. Indeed all attempts to locate on the potential energy surface (PES) a $[\text{Cu}^{\text{II}}(\text{capca})(\text{O}_2)]^+$ complex with O₂ coordinated to Cu(II) in either an end-on or a side-on coordination mode were not successful. Using as starting geometries for possible $[\text{Cu}^{\text{II}}(\text{capca})(\text{O}_2)]^+$ adducts involving coordination of dioxygen to Cu(II) metal center either in an end-on or a side-on coordination mode the optimization procedures pushed dioxygen to dissociation. No local minimum corresponding to 1:1 Cu^{II}:O₂ adducts formulated as $[\text{Cu}^{\text{II}}(\text{capca})(\text{O}_2)]^+$ was found even in some cases solving the SCF convergence problems. Coordination of O₂ to Cu(II) center in complex **2'** could not be supported by the nature of the FMOs and the natural atomic charge distribution of the complex **2'** (Fig. S2). The SOMO and LUMO of complex **2'** are mainly localized on the N(3)-C(13) bond [20.1% on N(3) and 4.8% on C(13) and 14.3% on N(3) and 23.1% on C(13) respectively]. Therefore, the interaction of

the π_{1g}^* -HOMO of $^3\text{O}_2$ with the SOMO and LUMO of **2'** is localized on the N(3)-C(13) bond yielding the $[\text{Cu}^{\text{II}}(\text{capca-O}_2)]^+$ intermediate shown in Fig. 11.

In $[\text{Cu}^{\text{II}}(\text{capca-O}_2)]^+$ the dioxygen has been activated and transformed to a peroxy group with the O-O bond distance of 1.447 Å (estimated Wiberg Bond Index, WBI = 0.982) being longer than the O-O bond distance of 1.423 Å in H_2O_2 (WBI = 1.014) calculated at the same level of theory. The O(2) of the peroxy moiety forms a weak N(3)-O(2) bond with a bond length of 1.469 Å (WBI = 0.917) while O(2') forms a slightly stronger C(13)-O(2') bond with a bond length of 1.433 Å (WBI = 0.931) (Fig. 11). The estimated WBI for the N(3)-C(13) bond is 0.939 indicates a remarkable weakening of the N(3)-C(13) bond compared to the N(3)-C(13) bond of the complex **2'** having a WBI value of 1.664.

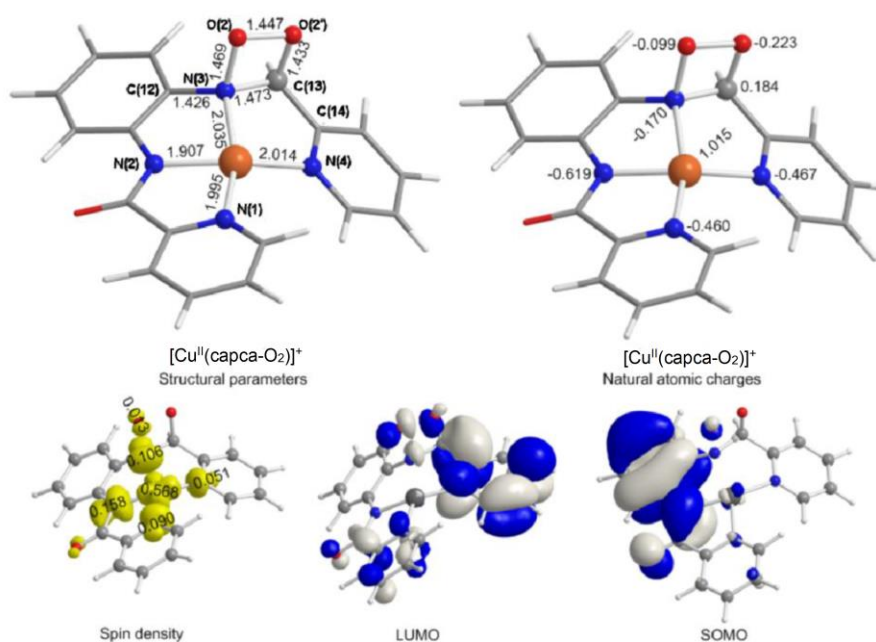


Fig. 11 Selected structural parameters, natural atomic charges, and Frontier Molecular Orbitals (FMOs) and the 3D plots of the spin density (isosurface = 0.002), calculated at the PBE0/def2-TZVP level in methyl alcohol solution (arbitrary numbering), of the complex intermediate $[\text{Cu}^{\text{II}}(\text{capca-O}_2)]^+$.

The interaction of the peroxy group with the N(3)-C(13) moiety of the ligand capca⁻ introduces remarkable structural changes into the complex **2'**. The Cu^{II}-N(3) distance is elongated by 0.059 Å with respect to the corresponding distance in complex **2'**, while the Cu^{II}-N(4), Cu^{II}-N(1) and Cu^{II}-N(2) coordination bonds are shortened by 0.040, 0.019 and 0.021 Å respectively (Fig. 11 and Table 1). Noteworthy are the significant weakening of the N(3)-C(13) and N(3)-C(12) bonds which are elongated by 0.198 and 0.037 Å respectively. Charge transfer of natural atomic charge towards dioxygen took place in [Cu^{II}(capca-O₂)]⁺ intermediate amounted to -0.322 |e|, which was distributed on the O(2) (-0.099 |e|) and O(2') (-0.223 |e|) oxygen atoms. Perusal of the 3D plots of the Mulliken spin density distribution in **2'** (Fig. S2) and [Cu^{II}(capca-O₂)]⁺ (Fig. 11) shows that a fraction of spin density amounted to 0.128 and 0.106 au is transferred to N(3) respectively. In [Cu^{II}(capca-O₂)]⁺ intermediate the O(2) of the peroxy moiety acquires also a small amount (0.013 au) (Fig. 11) of spin density giving to the coordinated peroxy moiety a radical character. The copper metal center in [Cu^{II}(capca-O₂)]⁺ intermediate keeps its oxidation state to II. The natural atomic charges on copper(II) central atoms in **2'** ($Q_{\text{Cu}} = 1.026$ |e|) and [Cu^{II}(capca-O₂)]⁺ ($Q_{\text{Cu}} = 1.015$ |e|) remain practically unchanged.

In the next step [Cu^{II}(capca-O₂)]⁺ intermediate reacts with either CH₃OH or H₂O (Fig. 12) to afford **5** or **5'** and nitroso(pyridin-2-yl)methanol, PyCH(OH)(NO), via an exothermic process with predicted exothermicities of 26.1 and 23.4 kcal/mol respectively (Fig. 12). Subsequently, the nitroso(pyridin-2-yl)methanol is transformed to the more stable (by 2.0 kcal/mol) 2-(nitromethyl)pyridine, PyCH₂(NO₂) isomer. The alternative PyCH(NO₂H) tautomer was found to be less stable than PyCH₂(NO₂) by 8.2 kcal/mol.

The $\text{PyCH}_2(\text{NO}_2)$ isomer contains an active methylene group and in the presence of a base (B) is easily deprotonated yielding the $[\text{PyCH}(\text{NO}_2)]^-$ nucleophile (Fig. 12). The estimated proton affinity of the $[\text{PyCH}(\text{NO}_2)]^-$ nucleophile is 188.6 kcal/mol at the PBE0/def2-TZVP level in methyl alcohol solution.

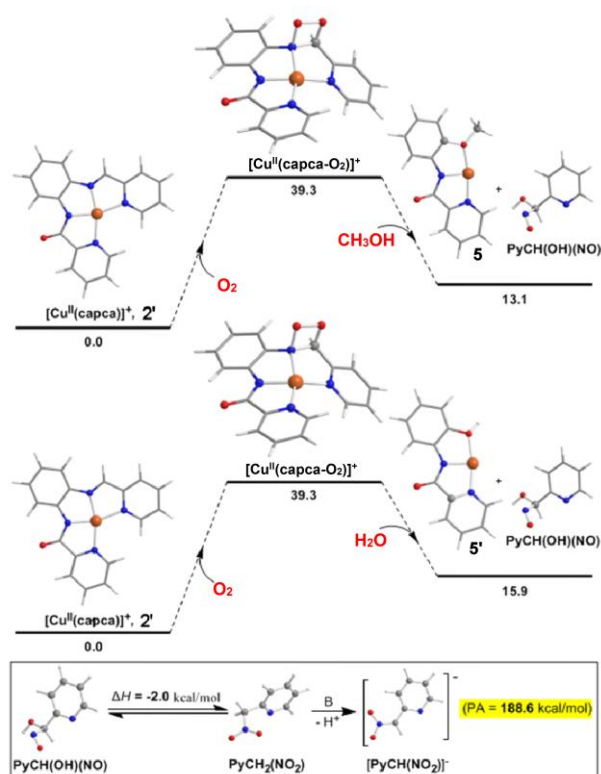


Fig. 12. Geometric and energetic profile of oxidation by air of **2'**, calculated at the PBE0/def2-TZVP level in methyl alcohol solution.

Next the $[\text{PyCH}(\text{NO}_2)]^-$ nucleophile attacks the C(13) electrophilic center ($Q_{\text{C}(2)} = 0.143 \text{ |e|}$) of the complex **2'** yielding intermediate **Im1** (Fig. 13) with an energy demand of 11.2 kcal/mol. **Im1** surmounting an energy of 5.3 kcal/mol releases the pyridine yielding intermediate **A**, which is transformed to the final product **B** (see Scheme 6). Species **B** is more stable than **A** by 2.7 kcal/mol. It is obvious that two **B**'s are combined in CH_3OH solution to give the dinuclear compound **4** (see Scheme 6).

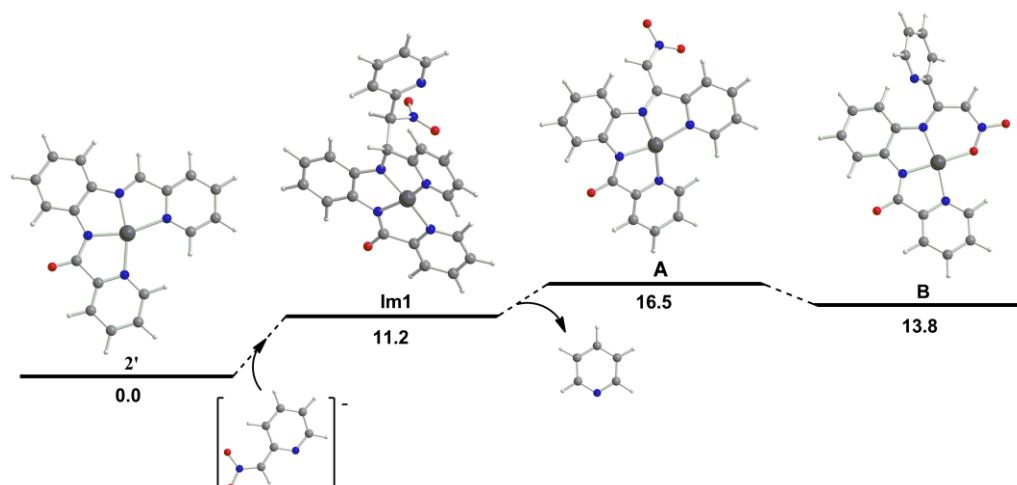
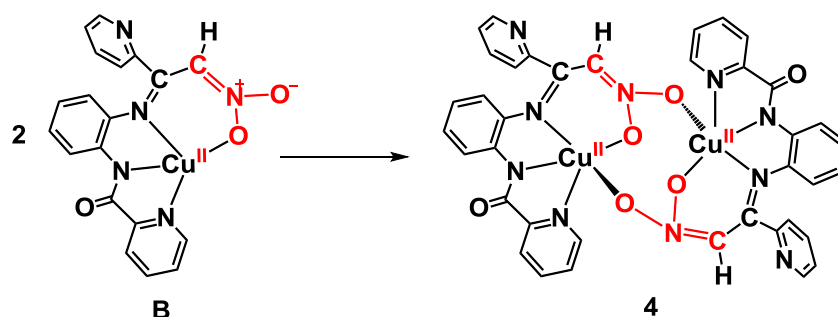


Fig. 13 Geometric and energetic profile of the aza-Henry reaction of complex **2'**, with the $[\text{PyCH}(\text{NO}_2)]^-$ nucleophile calculated at the PBE0/def2-TZVP level in methyl alcohol solution.



Scheme 6 Combination of two species **B** in CH_3OH to obtain the dinuclear compound **4**.

The reason for the synthesis of ligand Hmcapa

To unambiguously prove that the site of interaction of dioxygen with $[\text{Cu}^{\text{II}}(\text{capca})]^+$ is indeed the $>\text{C}=\text{N}-$ group and not the copper(II) atom the ligand Hmcapa (Scheme 1) was synthesized in which the methyl group was substituted for the hydrogen atom of the imino group. The design of the ligand Hmcapa was based on: i) the bigger methyl group would induce steric hindrance and ii) the electrophilic carbon atom of the imine group is getting less electrophilic due to electron-releasing effect of the methyl group (+I effect).

Gratifyingly, the complex $[\text{Cu}^{\text{II}}(\text{mcapca})]^+$ was stable under dioxygen as it was proved by UV-vis, c.w. EPR and ESI-MS spectroscopies in marked contrast to $[\text{Cu}^{\text{II}}(\text{capca})]^+$.

This makes crystal-clear that the site of activation of dioxygen is the ligand and not the copper(II) atom. In line with the experimental data, theory also predicts that the interaction of $[\text{Cu}^{\text{II}}(\text{mcapca})]^+$ with dioxygen to form the $[\text{Cu}^{\text{II}}(\text{mcapca}-\text{O}_2)]^+$ species demands a higher energy barrier by 2.1 kcal/mol in comparison with species $[\text{Cu}^{\text{II}}(\text{capca})]^+$.

Conclusions

In conclusion, a series of mononuclear and a dinuclear azinate copper(II) compounds with three biologically relevant amidate ligands was synthesized, structurally and physicochemically characterized. The ligated to the copper(II) secondary amine group of the complex $[\text{Cu}^{\text{II}}(\text{Hcapcah})]^+$ in methyl alcohol is oxidized by air in a stepwise fashion to imine, giving the complex $[\text{Cu}^{\text{II}}(\text{capca})]^+$, and the ligated imine group of it is oxidized to copper(II)-azinate species **B** (Fig. 13 and Scheme 6). Theoretical calculations for the system $[\text{Cu}^{\text{II}}(\text{capca})]^+/\text{O}_2$, supported by c. w. EPR measurements, proved that the imine copper(II) complex **2**·CH₃OH is able to activate dioxygen by direct attack of it to the ligated to copper(II) organic substrate. Apparently this study supports that the coordination of O₂ to the copper ion is not mandatory in order the copper complexes (enzymes or model species) to exhibit oxidases' or oxygenases' activity.

Conflicts of interest

There are no conflicts to declare.

Acknowledgements

The authors acknowledge the financial support by the Research Promotional Foundation (RPF) of Cyprus and the European Structural Funds ANABAΘΜΙΣΗ/ΠΙΛΓΙΟ/0308/32, the Unit ORBITRAP-LC-MS as well as Prof.Dr. Spyros Perlepes and Professor Leroy (Lee) Cronin.

Author Contributions

The manuscript was written through contributions of all authors. All authors have given approval to the final version of the manuscript.

[§]The designated authors have contributed equally.

References

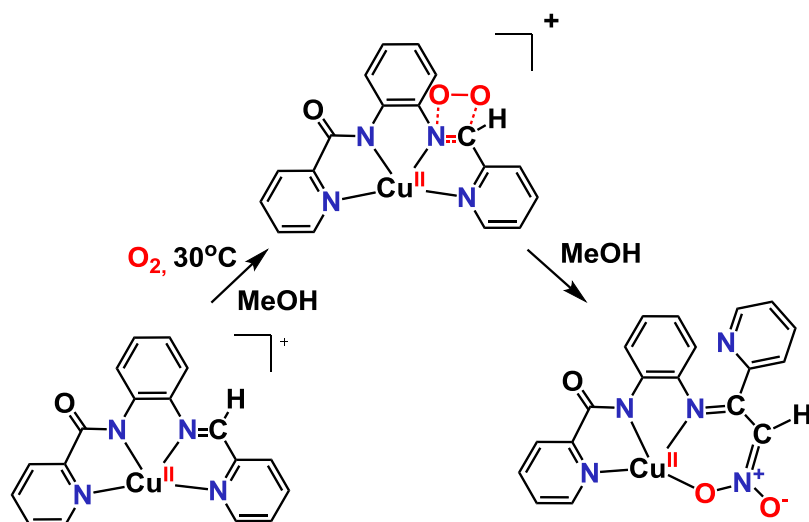
1. A. Bakac, *Inorg. Chem.*, 2010, **49**, 3584-3593.
2. C. E. Elwell, N. L. Gagnon, B. D. Neisen, D. Dhar, A. D. Spaeth, G. M. Yee and W. B. Tolman, *Chem. Rev.*, 2017, **117**, 2059-2107.
3. A. T. Fiedler and A. A. Fischer, *J. Biol. Inorg. Chem.*, 2017, **22**, 407-424.
4. S. Sahu and D. P. Goldberg, *J. Am. Chem. Soc.*, 2016, **138**, 11410-11428.
5. G. M. Yee and W. B. Tolman, *Journal*, 2015, **15**, 131-204.
6. X. Engelmann, S. Yao, E. R. Farquhar, T. Szilvási, U. Kuhlmann, P. Hildebrandt, M. Driess and K. Ray, *Angewandte Chemie - International Edition*, 2017, **56**, 297-301.
7. D. E. DeRosha, B. Q. Mercado, G. Lukat-Rodgers, K. R. Rodgers and P. L. Holland, *Angewandte Chemie - International Edition*, 2017, **56**, 3211-3215.
8. D. Munz and T. Strassner, *Inorg. Chem.*, 2015, **54**, 5043-5052.
9. A. Panja, N. C. Jana, S. Adak and K. Pramanik, *Inorg. Chim. Acta*, 2017, **459**, 113-123.
10. J. Sun, Z. Ou, R. Guo, Y. Fang, M. Chen, Y. Song and K. M. Kadish, *J. Porphyrins Phthalocyanines*, 2016, **20**, 456-464.
11. Y. Isaka, S. Kato, D. Hong, T. Suenobu, Y. Yamada and S. Fukuzumi, *Journal of Materials Chemistry A*, 2015, **3**, 12404-12412.
12. M. Stylianou, C. Drouza, J. Giapintzakis, G. I. Athanasopoulos and A. D. Keramidas, *Inorg. Chem.*, 2015, **54**, 7218-7229.
13. M. O. Ross and A. C. Rosenzweig, *J. Biol. Inorg. Chem.*, 2017, **22**, 307-319.
14. J. J. Liu, D. E. Diaz, D. A. Quist and K. D. Karlin, *Isr. J. Chem.*, 2016, **56**, 738-755.
15. C. A. Ramsden and P. A. Riley, *Bioorg. Med. Chem.*, 2014, **22**, 2388-2395.
16. M. Wikström, *Biochimica et Biophysica Acta - Bioenergetics*, 2012, **1817**, 468-475.
17. V. J. Klema and C. M. Wilmot, *International Journal of Molecular Sciences*, 2012, **13**, 5375-5405.
18. A. C. Rosenzweig and M. H. Sazinsky, *Current Opinion in Structural Biology*, 2006, **16**, 729-735.
19. A. Decker and E. I. Solomon, *Curr. Opin. Chem. Biol.*, 2005, **9**, 152-163.
20. E. A. Lewis and W. B. Tolman, *Chem. Rev.*, 2004, **104**, 1047-1076.
21. L. M. Mirica, X. Ottenwaelder and T. D. P. Stack, *Chem. Rev.*, 2004, **104**, 1013-1045.

22. E. I. Solomon, D. E. Heppner, E. M. Johnston, J. W. Ginsbach, J. Cirera, M. Qayyum, M. T. Kieber-Emmons, C. H. Kjaergaard, R. G. Hadt and L. Tian, *Chem. Rev.*, 2014, **114**, 3659-3853.
23. S. Itoh, in *Copper-Oxygen Chemistry*, eds. K. D. Karlin and S. Itoh, John Wiley & Sons, Hoboken, 2011, vol. 4, ch. 225–282.
24. C. E. Elwell, N. L. Gagnon, B. D. Neisen, D. Dhar, A. D. Spaeth, G. M. Yee and W. B. Tolman, *Chem. Rev.*, 2017, **117**, 2059-2107.
25. D. A. Quist, D. E. Diaz, J. J. Liu and K. D. Karlin, *J. Biol. Inorg. Chem.*, 2017, **22**, 253-288.
26. C. Würtele, E. Gaoutchenova, K. Harms, M. C. Holthausen, J. Sundermeyer and S. Schindler, *Angewandte Chemie - International Edition*, 2006, **45**, 3867-3869.
27. D. Maiti, J. S. Woertink, M. A. Vance, A. E. Milligan, A. A. Narducci Sarjeant, E. I. Solomon and K. D. Karlin, *J. Am. Chem. Soc.*, 2007, **129**, 8882-8892.
28. R. L. Peterson, R. A. Himes, H. Kotani, T. Suenobu, L. Tian, M. A. Siegler, E. I. Solomon, S. Fukuzumi and K. D. Karlin, *J. Am. Chem. Soc.*, 2011, **133**, 1702-1705.
29. J. Y. Lee, R. L. Peterson, K. Ohkubo, I. Garcia-Bosch, R. A. Himes, J. Woertink, C. D. Moore, E. I. Solomon, S. Fukuzumi and K. D. Karlin, *J. Am. Chem. Soc.*, 2014, **136**, 9925-9937.
30. K. Fujisawa, M. Tanaka, Y. Moro-oka and N. Kitajima, *J. Am. Chem. Soc.*, 1994, **116**, 12079-12080.
31. A. Kunishita, M. Kubo, H. Sugimoto, T. Ogura, K. Sato, T. Takui and S. Itoh, *J. Am. Chem. Soc.*, 2009, **131**, 2788-2789.
32. P. J. Donoghue, A. K. Gupta, D. W. Boyce, C. J. Cramer and W. B. Tolman, *J. Am. Chem. Soc.*, 2010, **132**, 15869-15871.
33. A. Kunishita, M. Z. Ertem, Y. Okubo, T. Tano, H. Sugimoto, K. Ohkubo, N. Fujieda, S. Fukuzumi, C. J. Cramer and S. Itoh, *Inorg. Chem.*, 2012, **51**, 9465-9480.
34. Y. Kobayashi, K. Ohkubo, T. Nomura, M. Kubo, N. Fujieda, H. Sugimoto, S. Fukuzumi, K. Goto, T. Ogura and S. Itoh, *Eur. J. Inorg. Chem.*, 2012, DOI: 10.1002/ejic.201200177, 4574-4578.
35. M. F. Qayyum, R. Sarangi, K. Fujisawa, T. D. P. Stack, K. D. Karlin, K. O. Hodgson, B. Hedman and E. I. Solomon, *J. Am. Chem. Soc.*, 2013, **135**, 17417-17431.
36. S. Kim, J. Y. Lee, R. E. Cowley, J. W. Ginsbach, M. A. Siegler, E. I. Solomon and K. D. Karlin, *J. Am. Chem. Soc.*, 2015, **137**, 2796-2799.
37. D. A. Iovan, A. T. Wrobel, A. A. McClelland, A. B. Scharf, G. A. Edouard and T. A. Betley, *Chem. Commun.*, 2017, **53**, 10306-10309.
38. C. Citek, J. B. Gary, E. C. Wasinger and T. D. P. Stack, *J. Am. Chem. Soc.*, 2015, **137**, 6991-6994.
39. C. Citek, S. Herres-Pawlis and T. D. P. Stack, *Acc. Chem. Res.*, 2015, **48**, 2424-2433.
40. C. Citek, C. T. Lyons, E. C. Wasinger and T. D. P. Stack, *Nature Chemistry*, 2012, **4**, 317-322.
41. J. B. Gary, C. Citek, T. A. Brown, R. N. Zare, E. C. Wasinger and T. D. P. Stack, *J. Am. Chem. Soc.*, 2016, **138**, 9986-9995.
42. B. D. Neisen, N. L. Gagnon, D. Dhar, A. D. Spaeth and W. B. Tolman, *J. Am. Chem. Soc.*, 2017, **139**, 10220-10223.
43. W. Keown, J. B. Gary and T. D. P. Stack, *J. Biol. Inorg. Chem.*, 2017, **22**, 289-305.
44. K. Yoshizawa, *Bull. Chem. Soc. Jpn.*, 2013, **86**, 1083-1116.
45. A. De La Lande, D. R. Salahub, J. Maddaluno, A. Scemama, J. Pilme, O. Parisel, H. Gerard, M. Caffarel and J. P. Piquemal, *J. Comput. Chem.*, 2011, **32**, 1178-1182.
46. C. J. Cramer, W. B. Tolman, K. H. Theopold and A. L. Rheingold, *Proceedings of the National Academy of Sciences of the United States of America*, 2003, **100**, 3635-3640.

47. N. W. Aboelella, E. A. Lewis, A. M. Reynolds, W. W. Brennessel, C. J. Cramer and W. B. Tolman, *J. Am. Chem. Soc.*, 2002, **124**, 10660-10661.
48. Y. Lee and L. M. Sayre, *J. Am. Chem. Soc.*, 1995, **117**, 11823-11828.
49. Y. Lee and L. M. Sayre, *J. Am. Chem. Soc.*, 1995, **117**, 3096-3105.
50. B. J. Johnson, E. T. Yukl, V. J. Klema, J. P. Klinman and C. M. Wilmot, *J. Biol. Chem.*, 2013, **288**, 28409-28417.
51. M. Mure, S. A. Mills and J. P. Klinman, *Biochemistry*, 2002, **41**, 9269-9278.
52. C. M. Wilmot, J. Hajdu, M. J. McPherson, P. F. Knowles and S. E. V. Phillips, *Science*, 1999, **286**, 1724-1728.
53. Y. Liu, A. Mukherjee, N. Nahumi, M. Ozbil, D. Brown, A. M. Angeles-Boza, D. M. Dooley, R. Prabhakar and J. P. Roth, *J. Phys. Chem. B*, 2013, **117**, 218-229.
54. T. Murakawa, H. Hayashi, T. Sunami, K. Kurihara, T. Tamada, R. Kuroki, M. Suzuki, K. Tanizawa and T. Okajima, *Acta Crystallogr. Sect. D. Biol. Crystallogr.*, 2013, **69**, 2483-2494.
55. A. Noguchi, T. Kitamura, H. Onaka, S. Horinouchi and Y. Ohnishi, *Nature Chemical Biology*, 2010, **6**, 641-643.
56. Y. J. Sun, P. Li, Q. Q. Huang, J. J. Zhang and S. Itoh, *Eur. J. Inorg. Chem.*, 2017, **2017**, 1845-1854.
57. R. A. Steiner, K. H. Kalk and B. W. Dijkstra, *Proceedings of the National Academy of Sciences of the United States of America*, 2002, **99**, 16625-16630.
58. A. M. Morris, C. G. Pierpont and R. G. Finke, *Inorg. Chem.*, 2009, **48**, 3496-3498.
59. A. M. Morris, C. G. Pierpont and R. G. Finke, *J. Mol. Catal. A: Chem.*, 2009, **309**, 137-145.
60. Á. Dancs, N. V. May, K. Selmeczi, Z. Darula, A. Szorcsik, F. Matyuska, T. Páli and T. Gajda, *New J. Chem.*, 2017, **41**, 808-823.
61. C. Drouza and A. D. Keramidas, *Inorg. Chem.*, 2008, **47**, 7211-7224.
62. B. D. Neisen, N. L. Gagnon, D. Dhar, A. D. Spaeth and W. B. Tolman, *J. Am. Chem. Soc.*, 2017, **139**, 10220-10223.
63. E. J. Tolis, V. I. Teberekidis, C. P. Raptopoulou, A. Terzis, M. P. Sigalas, Y. Deligiannakis and T. A. Kabanos, *Chemistry - A European Journal*, 2001, **7**, 2698-2710.
64. G. R. Hanson, T. A. Kabanos, A. D. Keramidas, D. Mentzafos and A. Terzis, *Inorg. Chem.*, 1992, **31**, 2587-2594.
65. A. D. Keramidas, A. B. Papaioannou, A. Vlahos, T. A. Kabanos, G. Bonas, A. Makriyannis, C. P. Raptopoulou and A. Terzis, *Inorg. Chem.*, 1996, **35**, 357-367.
66. A. W. Addison, T. N. Rao, J. Reedijk, J. Van Rijn and G. C. Verschoor, *J. Chem. Soc., Dalton Trans.*, 1984, DOI: 10.1039/DT9840001349, 1349-1356.
67. S. L. Jain, P. Bhattacharyya, H. L. Milton, A. M. Z. Slawin, J. A. Crayston and J. D. Woollins, *Dalton Transactions*, 2004, 862-871.
68. J. Wang, B. Djukic, J. Cao, A. Alberola, F. S. Razavi and M. Pilkington, *Inorg. Chem.*, 2007, **46**, 8560-8568.
69. N. J. Hurley, J. J. Hayward, J. M. Rawson, M. Murrie and M. Pilkington, *Inorg. Chem.*, 2014, **53**, 8610-8623.
70. M. Bonamico, G. Dessy, V. Fares and L. Scaramuzza, *Cryst. Struct. Commun.*, 1976, **5**, 387-392.
71. K. V. Deuten and G. Klar, *Cryst. Struct. Commun.*, 1980, **9**, 479-486.
72. T. A. B. M. Bolsman and J. A. Van Doorn, *J. Organomet. Chem.*, 1979, **178**, 381-391.
73. J. Peisach and W. E. Blumberg, *Arch. Biochem. Biophys.*, 1974, **165**, 691-708.
74. G. Speier, A. M. Whalen, J. Csihony and C. G. Pierpont, *Inorg. Chem.*, 1995, **34**, 1355-1360.

75. N. Bartalucci, M. Bortoluzzi, F. Marchetti, G. Pampaloni, S. Schoch and S. Zacchini, *New J. Chem.*, 2017, **41**, 4329-4340.

Synopsis



Novel Cu^{II} complexes with the biologically relevant tetradentate amidate ligands, have been synthesized and physicochemically characterized. These complexes constitute the first precedent of a direct activation of dioxygen by a ligated to Cu^{II} $-HC=N-$ group, with implications for copper oxidases' and oxygenases' mechanisms.